Journal of Power Sources 220 (2012) 138–146

Contents lists available at SciVerse ScienceDirect

Journal of Power Sources

journal homepage: www.elsevier.com/locate/jpowsour

Novel mixed matrix membranes for sulfur removal and for fuel cell applications

Ligang Lin [a,b,*], Andong Wang [b], Longhui Zhang [b], Meimei Dong [b], Yuzhong Zhang [a,b]

[a] State Key Laboratory of Hollow Fiber Membrane Materials and Processes, Tianjin Polytechnic University, BInshuixidao 399, Tianjin 300387, PR China
[b] School of Materials Science and Engineering, Tianjin Polytechnic University, Tianjin 300387, PR China

HIGHLIGHTS

- Membranes are proposed for sulfur-free hydrogen source of fuel cell.
- Membrane performance is markedly related with three-dimensional transport channels.
- Two regeneration modes are proposed for separation of organic mixtures by MMMs.

GRAPHICAL ABSTRACT

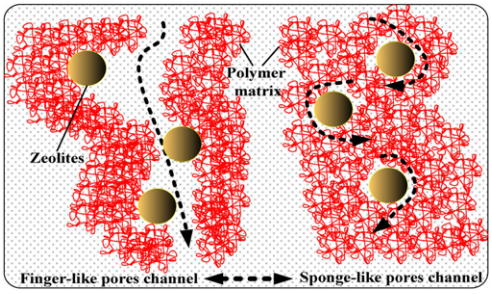

ARTICLE INFO

Article history:
Received 11 June 2012
Received in revised form
26 July 2012
Accepted 30 July 2012
Available online 8 August 2012

Keywords:
MMMs
Sulfur
Adsorption
Zeolites
Fuel cell

ABSTRACT

Sulfur removal is significant for fuels used as hydrogen source for fuel cell applications and to avoid sulfur poisoning of therein used catalysts. Novel mixed matrix membranes (MMMs) with well-defined transport channels are proposed for sulfur removal. MMMs are fabricated using polyimide (PI) as matrix material and Y zeolites as adsorptive functional materials. The influence of architecture conditions on the morphology transition from finger-like to sponge-like structure and the "short circuit" effect are investigated. The adsorption and regeneration behavior of MMMs is discussed, combining the detailed analysis of FT-IR, morphology, XPS, XRD and thermal properties of MMMs, the process-structure-function relationship is obtained. The results show that the functional zeolites are incorporated into three-dimensional network and the adsorption capacity of MMMs comes to 8.6 and 9.5 mg S g^{-1} for thiophene and dibenzothiophene species, respectively. And the regeneration behavior suggests that the spent membranes can recover about 88% and 96% of the desulfurization capacity by solvent washing and thermal treating regeneration, respectively. The related discussions provide some general suggestions in promoting the novel application of MMMs on the separation of organic–organic mixtures, and a potential alternative for the production of sulfur-free hydrogen source for fuel cell applications.

1. Introduction

During recent years, sulfur removal from hydrocarbon fuels has attracted lots of research interest. Hydrocarbon fuels are ideal hydrogen source of fuel cells, which is one of the most promising and convenient energy conversion devices for generating electricity for both mobile vehicles and stationary power plants including residential applications. However, the liquid hydrocarbon fuels usually contain certain sulfur compounds which are poisonous to both the catalysts used in fuel processor (such as reforming catalysts and water-gas-shift catalysts in hydrocarbon-based fuel cell system) and the electrode (anode) catalysts in fuel cell stack. Thus, the sulfur compounds in the liquid hydrocarbons fuels need to be reduced to less than 0.1 ppmw [1,2].

* Corresponding author. State Key Laboratory of Hollow Fiber Membrane Materials and Processes, Tianjin Polytechnic University, BInshuixidao 399, Tianjin 300387, PR China. Tel.: +86 22 83955808; fax: +86 22 83955055.
E-mail address: phdlinligang@yahoo.com.cn (L. Lin).

0378-7753/$ – see front matter © 2012 Elsevier B.V. All rights reserved.
http://dx.doi.org/10.1016/j.jpowsour.2012.07.086

Considering the inevitable octane number loss and tough operating conditions, it is difficult for the conventional hydrotreating desulfurization approach to achieve ultra low sulfur from cost and efficiency concerns [3]. Under above circumstances, quite a number of novel desulfurization methods have emerged, including oxidation, extraction, biodesulfurization, and adsorption, etc [4–6]. Among those processes, the adsorption approach is rather attractive, because it does not need to consume H_2 and can be operated at ambient temperature and pressure. However, the now developed adsorption desulfurization process is usually in fixed bed or fluid bed operation. During those operation circumstances, the leakage of absorbent particles with flowing fuel is inevitable. To prevent the leakage of particles, the size of used absorbent particle is usually requested at larger level, which means lower specific surface and undesirable adsorption efficiency.

Fortunately, the membrane technology, which has attracted considerable attention during recent years owing to its efficiency, ease of implementation and cost effectiveness, provides a competitive alternative over traditional separation techniques [7]. In current work, the novel mixed matrix membranes (MMMs) are proposed for sulfur removal from hydrocarbon fuels. MMMs are normally defined as the incorporation of an inorganic (dispersed) phase into a continuous polymer matrix. The incorporation of nanoporous inorganic adsorptive materials such as zeolites into polymeric membranes has attracted much attention, since which can combine the size/shape selectivity of nanoporous materials with the processability and mechanical stability of polymer [8]. Research interest has grown because MMMs are promising in improving membrane separation properties, and the recent attempts focus on gas separation, protein recovery and direct methanol fuel cell, etc [9–12].

However, until recently the report about the separation of organic–organic mixtures by MMMs is quite insufficient. Most liquid pairs in this category are of industrial importance. The challenge is how to fabricate well-defined transport channels for high selectivity and suitable flux. The transport of organic–organic liquid mixtures in MMMs is different with those gas pairs reported considerably during past several years [13]. Due to the pervasive flow and diffusion of gas molecules, considerable efforts for the fabrication of MMMs for gas separation focused on the design and control of organic–inorganic interface defects to achieve high performance. For the fabrication of MMMs for organic–organic mixtures, solvent resistant matrix and optimized microporous channels for sufficient contraction between liquid stream and MMMs are especially significant. Hydrocarbon fuel, which is the research subject under discussion, is complex liquid mixture composed of hundreds of organic compounds. The functional zeolites particles are proposed to be incorporated into the PI matrix with super solvent resistance to obtain MMMs. When the liquid fuel passes through the MMMs, the sulfur compounds are expected to adsorbed onto the surface of functional particles embedded in polymer pores, hence the sulfur removal realizes. However, the transport properties of MMMs are strongly dependent on the microporous morphology. The channel optimization is significant in improving the transport efficiency of fuel molecules in MMMs for high adsorption performance. Detailed analysis of process-structure-function relationship of MMMs for sulfur removal from fuels can provide helpful general suggestions for related researchers.

In the present study, the MMMs will be prepared using PI as matrix material and various Y zeolites as adsorptive functional materials. In order to fabricate MMMs with well-defined transport channels, the transition of membrane morphology from finger-like to sponge-like structure will be investigated. The "short circuit" effect will be considered. The adsorption and regeneration behavior will be discussed, combining the detailed analysis of FT-IR, morphology, XPS, XRD and thermal properties of MMMs, the process-structure-function relationship can be obtained.

2. Experimental

2.1. Materials

NaY zeolites, used as a starting material for making modified zeolites, were purchased from QiLu Petrochemical Catalyst Plant (China). Thiophene and dibenzothiophene (typical sulfur species in fuel) were from Chengdu Kelong Chemical Reagent Corporation and Shouerfu Reagent Corporation, respectively. Typical hydrocarbons (*n*-heptane, *n*-octane, cyclohexane, 1-hexene and toluene) and precipitation medium (ethanol, isopropanol and *n*-butyl alcohol) were all from Tianjin Kemiou Chemical Reagent Corporation. Silver nitrate was from Tianjin Yingda Chemical Reagent Corporation. Other reagents were from Sinopharm Chemical Reagent Corporation (China). All chemicals used were of analytical reagent (A.R.) grade and used without further purification. The monomer of 3,3′,4,4′-benzophenonetetracarboxylic dianhydride (BTDA) was from Beijing Multi. Technology Co., Ltd, 4,4′-diamino-3,3′-dimethyldiphenylmethane (DMMDA) from Shanghai EMST Corporation. And the monomers were purified by recrystallization. *N*,*N*-Dimethylformamide and tetrahydrofuran was purified on distillation under reduced pressure.

2.2. Mixed matrix membrane preparation

AgY zeolites were prepared by liquid-phase ion-exchange process followed our previous work [14,15]. NaY particles were added to silver nitrate solution in a stirred vessel. The mixture was stirred for certain time. After the ion-exchange treatments, the samples were filtered, washed, and dried at 80 °C. The silver ion loaded zeolites were calcined at 400 °C for 3 h. The optimal preparation conditions for AgY were as follows: 0.15 mol L^{-1} of silver nitrate solution, 1.0 of Ag^+/Na^+ mole ratio, 5 h of ion-exchange time and 20 °C of ion-exchange temperature.

BTDA-DMMDA polyimide was prepared by a two-step solution-imidization route. The diamine was dissolved in DMF, and then the diamine was gradually added into the solution. The mole ratio and solid content of diamine/dianhydride mixture were 1:1 and 13 wt.%, respectively. The mixture reacted for 10 h at room temperature producing a viscous polyamic acid solution. The chemical imidization was carried out with acetic anhydride and pyridine at room temperature for 14 h. The reaction mixture was then added to ethanol solution. The precipitate was collected by filtration, washed with water, and dried in vacuo at 150 °C to obtain the solid of polyimides.

Certain contents of zeolites were dispersed into the mixed solvent of *N*,*N*-dimethylformamide and tetrahydrofuran in a stirred vessel. The mixture was stirred for 4 h and then sonicated for 0.5 h to break the clusters of particles and to assure the particles well dispersed. Then PEG-400 was added to the mixture in order to improve the membrane morphology. Finally, PI, which has been dried in a vacuum oven at 120 °C for 24 h, was gradually added to the mixture and stirred for 24 h to ensure complete dissolution of polymer. Before casting, the solution was degassed. All membranes were made by phase inversion technique. The evaporation time was at 0 min, 0.5 min, 1.5 min and 10 min for comparison experiments. The dope solution was cast on a glass plate and immersed into a precipitation bath (20 °C). Four kinds of precipitation medium including water, ethanol, isopropanol and *n*-butyl alcohol were used for various pores and channels. During this process, solvent exchange occurred and the solidified membrane formed

with porous structure. To ensure that all of the solvent in the membrane structure was removed, membranes were immersed in the precipitation bath for 24 h. All membranes were prepared with zeolites loadings of 40 wt.%.

2.3. Adsorption and regeneration experiments

All dynamic adsorption or breakthrough experiments were performed in a permeation cell made of stainless steel, and the membranes were supported on a porous titanium disc with an effective membrane area of 46.9 cm^2. The setup consisted of a low-flow liquid pump, feed tanks, and a heating element. Temperature was measured by a chromel–alumel thermocouple. A metering pump was used to drive the fuel into the permeation cell. In all cases, a predetermined constant flow rate of 32.8 mL h^{-1} was used. The adsorption experiments were conducted at 25 °C with 430 mg L^{-1} of inlet sulfur concentration level. When the fuel feed consisting of hydrocarbons and thiophenic sulfur compounds passed through the permeation cell, the sulfur concentration of the outlet solution was analyzed by Micro-Coulometric Analysis Instrument (Jiangsu, China).

Regeneration of spent MMMs was performed by solvent washing and thermal treating, respectively. For the solvent washing method, the ethanol was used as desorption agent was driven into the permeation cell at 65 °C. The sulfur concentration of washing solvent was analyzed using the sulfur analyzer at intervals until the concentration was stable. The adsorption capacity of regenerative MMMs was tested to compare with the fresh samples. The regeneration was repeated four times to investigate the practical application potential of MMMs. For the thermal treating method, the spent MMMs were calcined at 250 °C. The regeneration was also repeated four times. The adsorption capacity of regenerative MMMs was tested to compare with the fresh membrane samples.

2.4. Characterization

The infrared spectra of prepared MMMs were obtained by KBr method on a TENSOR37 FT-IR. The XPS spectra of chemical composition of MMMs were recorded by X-ray photoelectron spectroscopy (ThermoFisher K-alpha). X-ray diffraction (XRD) analysis was carried out using a Bruker AXS D8 Advance diffractometer. The surface and cross-section microscopic morphology of various membrane samples was characterized by field-emission scanning electron microscope (FE-SEM), carried out on Hitachi S-4800. Differential Scanning Caborimetry (DSC) analysis was performed on both the raw PI membranes and MMMs using NETZSCH STA 409 PC/PG. The samples were heated from 35 to 800 °C at a heating rate of 10 °C min^{-1}, under nitrogen atmosphere, with a nitrogen flow rate of 50 mL min^{-1}.

3. Results and discussion

3.1. FT-IR and XPS analysis

FT-IR spectra of prepared zeolites/PI MMMs are shown in Fig. 1. The band at 1774 cm^{-1} (characteristic imido I band) and 1717 cm^{-1} (characteristic imido II band) corresponds to the symmetrical and asymmetrical stretching vibrations of the two C=O groups at five-membered imine ring, respectively. The band at 1368 cm^{-1} can be ascribed to the stretching vibration of C–N group, which is characteristic imido III band. The characteristic imido IV band can also be found at 719 cm^{-1}, which corresponds to the deformation vibration of imine ring. From the spectra of Fig. 1, the peak appearing at 990–1010 cm^{-1}, which corresponds to the stretching

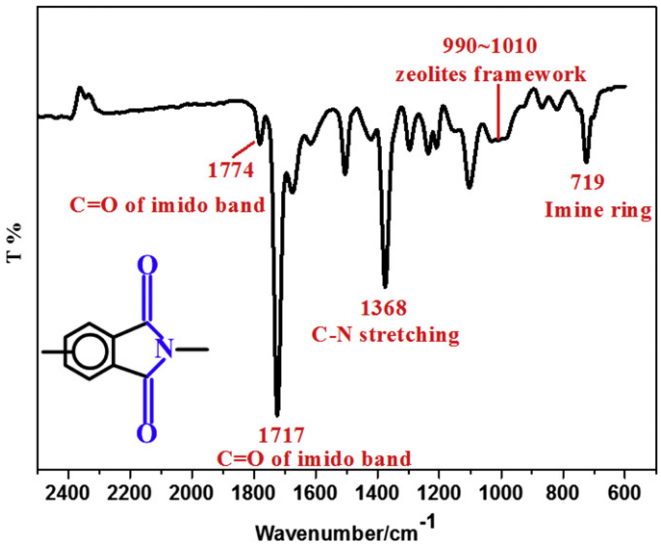

Fig. 1. FT-IR spectra of MMMs.

vibrations of the Y zeolites framework, demonstrates that the zeolites have been successfully immobilized into the PI base matrix.

The XPS results give more specific information of the surface chemical composition than the FT-IR. In Fig. 2, the strong XPS peaks can be clearly observed at 285.1 eV (C 1s), 400.1 eV (N 1s) and 531.9 eV (O 1s), which result from the imido groups of PI matrix. Also, for the MMMs, the peaks at 153.1 eV (Si 2s), 102.4 eV (Si 2p) and 76.9 eV (Al 2p) are assigned to the framework of incorporated Y zeolites. The peaks for Si and Al elements confirm the existence of zeolites on the MMMs surface. These findings are consistent with the IR (Fig. 1) and the following surface morphology (Fig. 3F) analysis, which indicates that the encapsulation is efficient.

3.2. Microporous channels optimization

The transport properties of MMMs are strongly dependent on the microporous morphology. The microporous channel optimization has been conducted by the detailed analysis and control of pore morphology transition, combining the investigation of practical performance.

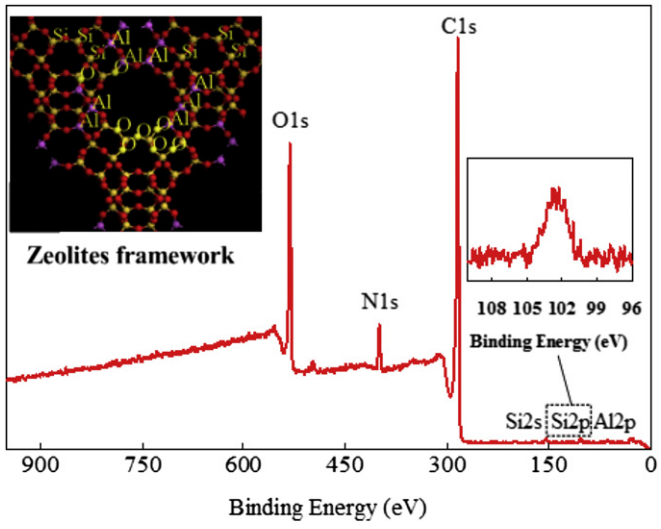

Fig. 2. XPS survey spectra of MMMs.

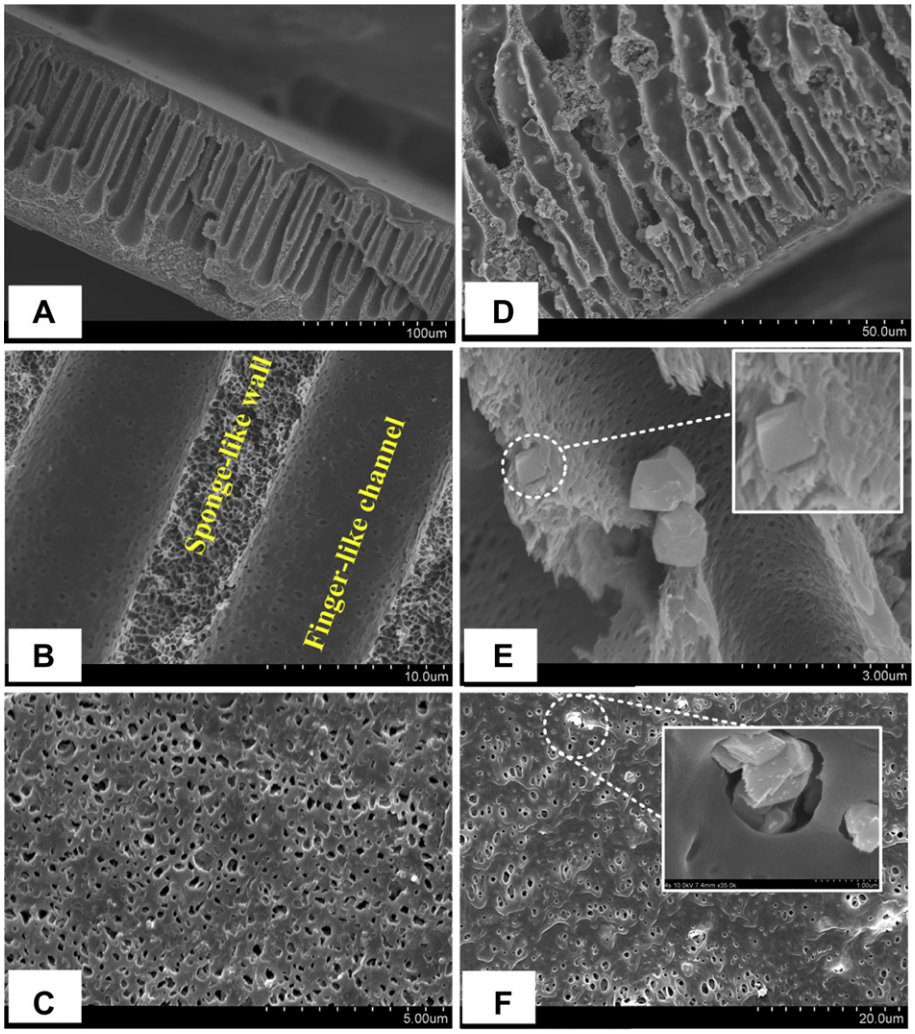

Fig. 3. FESEM images of raw PI membrane and MMMs: (A) raw PI membrane, cross-section, magnification ×400, (B) raw PI membrane, cross-section, magnification ×5000, (C) raw PI membrane, surface, magnification ×10 K, (D) MMMs, cross-section, magnification ×1000, (E) MMMs, cross-section, magnification ×15 K, (F) MMMs, surface, magnification ×2000.

3.2.1. Morphology analysis and "short circuit" effect

The cross-section and surface morphology at various magnifications of raw PI membrane and MMMs has been observed, and the FESEM images are shown in Fig. 3. Water was taken as precipitation medium and the evaporation time was at 0.5 min during preparation. It can be found from Fig. 3 that the raw PI membranes as well as the MMMs have abundant finger-like pores. The sponge-like pores exist in the wall between finger-like channels. By comparison analysis on the MMMs images with raw PI membranes in Fig. 3, the zeolites particles are dispersed and incorporated in the polymer matrix, and the particles can be found both in finger-like pore channels and sponge-like wall (Fig. 3E) as well as the surface pores (Fig. 3F). The existed surface pores provide places for the fuel in and out of MMMs. The conclusions are in good accordance with the FT-IR and XPS analysis. From the magnified images of surface pores and particles morphology (Fig. 3F), there are interface voids. Because of the different properties and the strong aggregation tendency between organic phase (polymer) and inorganic fillers, the detachment of polymer chains from the zeolites surface can cause the polymer–inorganic interface voids during MMMs fabrication. Unlike those MMMs for gas separation, the interface voids of MMMs for organic–organic liquid mixtures do not always mean defects. The interface voids can provide the necessary channels for liquid fuel flowing through.

However, the channels, especially the finger-like pores, are not ideal structure for the sulfur removal application under discussion. The "short circuit" effect can dramatically affects the adsorption performance of MMMs. The schematic diagram of various pore morphology of MMMs considering "short circuit" effect is shown in Fig. 4. From Fig. 4, the finger-like pore channels can not ensure the contact between the incorporated zeolites particles and the liquid fuel flowing through. In this case, fuel molecules pass through the less resistant by-pass preferably instead of passing through the particles, and thus the inorganic phase becomes unusable. Obviously, the sufficient contact between the incorporated zeolites and fuel is significant to achieve efficient adsorption. While for the sponge-like pore case, as shown in case II of Fig. 4, the polymer chains and the pore morphology are in favor of the direct contact between the incorporated zeolites and the liquid fuel flowing through.

To obtain well-defined transport channels and deep understanding of process-structure-function relationship of MMMs, the effects of preparation conditions such as precipitation medium and evaporation time on the morphology and adsorption performance will be discussed in the following section.

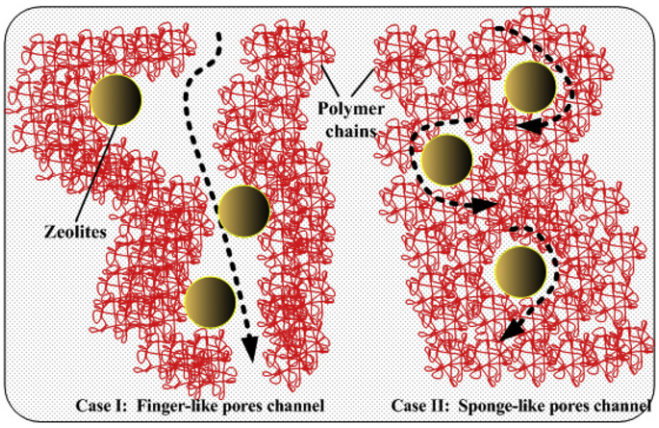

Fig. 4. The schematic diagram of various pore morphology of MMMs considering "short circuit" effect.

3.2.2. *Effect of precipitation medium*

Fig. 5 presents the cross-section morphology of MMMs with various precipitation medium during fabrication process. All the membranes in present study were made by phase inversion technique, as stated in the experimental section. The involved precipitation medium include water, ethanol, isopropanol and *n*-butyl alcohol. From the images of Fig. 5, cross-section structure transition from finger-like pores to sponge-like pores with the precipitation medium order of water, ethanol, isopropanol and *n*-butyl alcohol can be clearly seen. During phase-inversion process, when the dope solution was immersed into a precipitation bath, the solvent exchange with the precipitation medium (namely 'nonsolvent') occurs, hence the phase separation and precipitation begins. Through precipitation process, desolvation of the polymerphase converts the polymer to a relatively solid gel phase, which forms the matrix of the membranes. And the liquid solvent–nonsolvent phase forms the pores. The precipitation behavior, especially the exchange kinetics of solvent and nonsolvent, has significant influence on the pore morphology. Usually, depending on the rate of phase separation (demixing), two different structures, namely a sponge-like or a finger-like membrane configuration can be observed [16]. Instantaneous demixing occurs when the phase separation begins immediately after immersion. For instantaneous demixing process, a finger-like structure can be expected. However, for delayed demixing process, the composition of the entire solution remains in the homogeneous region of the phase diagram for a certain period of time, during which a sponge-like structure can usually be observed.

The viscosity of precipitation medium (Fig. 6A) and solubility parameter difference $\Delta\delta$ (Fig. 6B) between solvent and precipitation medium are used to analyze the precipitation behavior and pore morphology. From Fig. 6A, the viscosity of precipitation medium follows the order: water < ethanol < isopropanol < *n*-butyl alcohol. The higher viscosity of precipitation medium means the higher diffusion resistance during phase separation, hence the delayed demixing, which facilitates the transition to sponge-like structure. In the present study, *N*-methyl-pyrrolidone (NMP), which is typical polar solvent, is used as a primary dope solvent. From Fig. 6B, the $\Delta\delta$ between NMP and precipitation medium follows the order: water > ethanol > isopropanol > *n*-butyl alcohol, which is the reverse as that found for viscosity. The higher $\Delta\delta$ means the weaker solvation performance of precipitation medium, which is in favorable of the precipitation occurrence, hence the instantaneous demixing, which facilitates the transition to finger-like structure. The discussions correspond to the analysis on structure transition from finger-like pores to sponge-like pores (Fig. 5).

Practical performance of MMMs should taken into account for further structure optimization of MMMs. Table 1 shows the effect of preparation conditions of MMMs on adsorption performance and flux. It can be observed from Table 1 that the adsorption capacity increases with the following order of precipitation medium: *n*-butyl alcohol > isopropanol > ethanol > water, while is the reverse as that found for flux of MMMs. Obviously, the structure transition from finger-like to sponge-like is favorable for adsorption behavior due to the weakening "short circuit" effect and the enhanced contraction probability between the incorporated zeolites and fuel as revealed in Fig. 4. However, the entire sponge-like structure means higher transport resistance for fuel molecules to pass

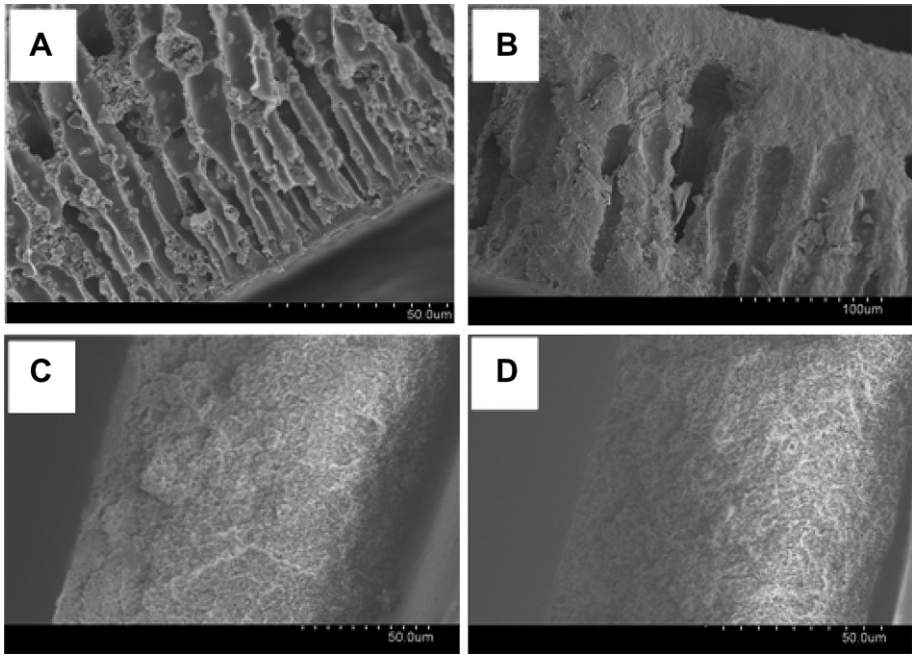

Fig. 5. FESEM images of cross-sections of MMMs at various precipitation medium: (A) water, (B) ethanol, (C) isopropanol and (D) *n*-butyl alcohol.

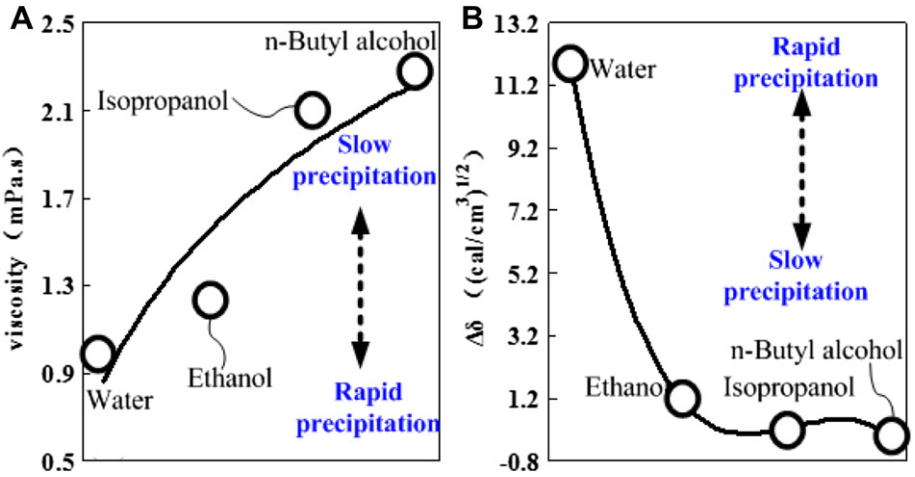

Fig. 6. The relationship between precipitation behavior and medium properties: (A) viscosity, (B) $\Delta\delta$ between solvent and precipitation medium.

through the matrix of MMMs, hence the lower flux. By detailed comparison analysis on the membrane performance and corresponding precipitation medium, the adsorption performance and flux of MMMs are both at relatively higher level with ethanol medium. The following further investigation of MMMs takes ethanol as precipitation medium.

3.2.3. *Effect of evaporation time*

For further structure tailoring and higher performance, the effect of evaporation time on MMMs has been investigated. The cross-section images of MMMs at various evaporation times are shown in Fig. 7, and the corresponding adsorption performance and flux in Table 1. Fig. 7 demonstrates the increasing thickness of skin layer and the clear transition of cross-section pore structure from finger-like to sponge-like with the increasing evaporation time. During membrane preparation process, the increasing evaporation time means the increasing polymer concentration of dope solution, which results in the increased mass transfer resistance for subsequent phase separation and precipitation process. As mentioned in the foregoing section, increased mass transfer resistance means delayed demixing and structure transition to sponge-like morphology, which are verified by the images in Fig. 7. When the evaporation time is prolonged to 10 min, the finger-like channels disappear, instead of by entire sponge-like pores. Table 1 gives the corresponding adsorption performance and flux of MMMs under various evaporation times. By detailed performance comparison, it is found that maintaining certain finger-like pores into the three-dimensional network structure of MMMs is favorable for higher flux. Relatively higher level of adsorption performance and flux of MMMs are both achieved at 1.5 min of evaporation time, which will be used in the following further investigations.

Table 1
The effect of preparation conditions of MMMs on adsorption performance and flux.

Preparation conditions		Adsorption capacity (mg S g^{-1})	Flux (L m^{-2} h^{-1})
Precipitation medium	Evaporation time (min)		
Water	0.5	6.2	43.6
Ethanol	0.5	7.9	19.8
Isopropanol	0.5	8.4	2.9
n-Butyl alcohol	0.5	8.8	2.4
Ethanol	0	7.5	26.7
Ethanol	1.5	8.6	12.9
Ethanol	10	–	0.0

3.3. *Adsorption behavior*

For further investigation on the practical performance of MMMs, a number of breakthrough studies have been carried out to discuss the adsorption behavior and sulfur removal performance.

The liquid fuel flowed through the MMMs and the sulfur concentrations in the effluent samples were monitored at intervals until the outlet sulfur concentration was stable. In all the cases, a predetermined constant flow rate of 32.8 mL h^{-1} was used. The breakthrough curves for the adsorptive removal of sulfur from the model fuel by MMMs are shown in Fig. 8. The experiments were conducted at 25 °C of feed temperature.

From Fig. 8, it is evident that the breakthrough of NaY/PI MMMs appears at the beginning outlet of fuel, while that of AgY/PI MMMs later. Approximately 14 g of fuel with 430 mg L^{-1} of inlet sulfur concentration is desulfurized to below 0.1 mg L^{-1} sulfur using 1 g of AgY/PI MMMs, which means that the outlet fuel can be used as sulfur-free hydrogen source for fuel cell applications. From Fig. 8, the outlet sulfur concentration increases firstly and then tends to stable. It is interesting to note that, in all cases, the outlet sulfur concentration can not reach the corresponding inlet sulfur level. In fact, when the fuel passes through the MMMs, the adsorption and desorption co-exist. During the adsorption process of sulfur compounds over MMMs, the hydrocarbons in fuel have certain desorption and regeneration effect, which can be verified by the solvent washing regeneration research in Section 3.4.

The distinct adsorption performance of MMMs embedded with different kinds of zeolites was markedly related with the binding force between sulfur compounds and the fillers. For NaY, its binding with sulfur is attributed to weak Van der Waals force (typical physical adsorption). Besides sulfur compounds, NaY also adsorbs hydrocarbon existing in the fuel, which would cause low adsorption selectivity for sulfur, hence the low desulfurization performance. For AgY, the high adsorption capacity for sulfur is obtained due to a particular π-complexation between the Ag^{+} ions and the thiophenic aromatic rings, which has been proven by Yang and his coworkers [17] The better adsorption performance of AgY/PI MMMs compared to NaY/PI MMMs could be due to the distinct adsorption mode: π-complexation is stronger binding force than Van der Waals force.

Hydrocarbon fuel is complex mixture composed of hundreds of organic compounds, in which four typical hydrocarbon groups are alkanes, cycloalkanes, aromatics and alkenes. According to the hydrocarbon groups content in actual fuel, which composed of

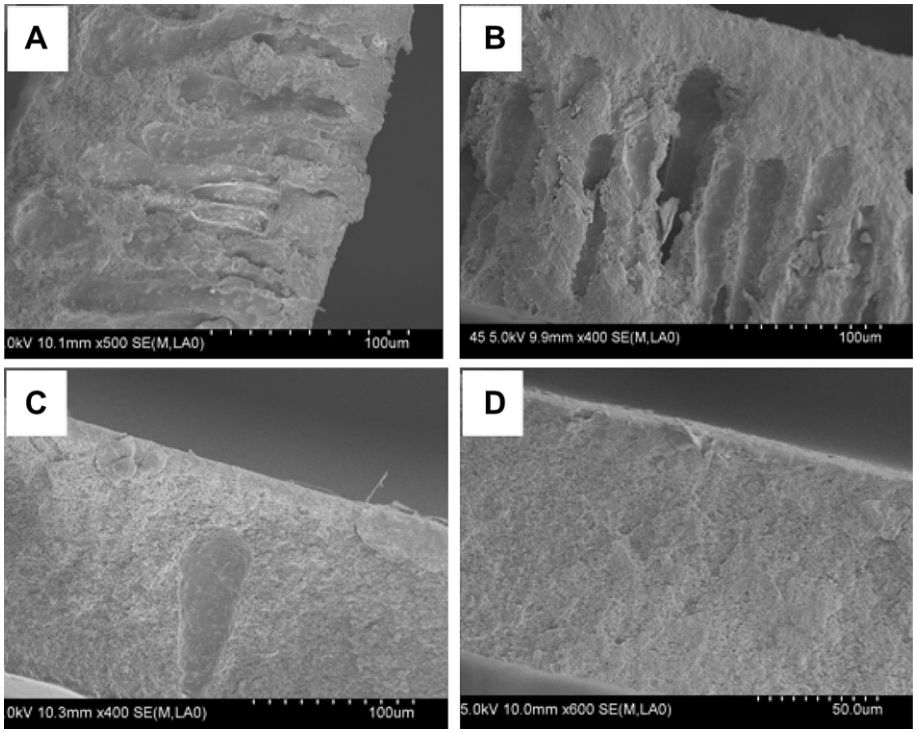

Fig. 7. FESEM of cross-sections of MMMs at various evaporation time: (A) 0 min, (B) 0.5 min, (C) 1.5 min and (D) 10 min.

alkanes (32.7 wt.%), cycloalkanes (9.8 wt.%), alkenes (40.0 wt.%) and aromatics (15.6 wt.%) [18], model fuel feed composed of various hydrocarbon groups was prepared and used for performance investigation. The influence of typical hydrocarbon components on adsorption behavior of MMMs is shown by the breakthrough curves in Fig. 9A and B. The experiments were conducted at 25 °C with 430 mg L^{-1} of inlet sulfur concentration. When the fuel feed consisting of hydrocarbons and thiophenic sulfur compounds passed through the MMMs, the outlet sulfur concentration was detected. For Fig. 9A case, the inlet fuel is composed of thiophene, *n*-heptane (35 wt.%), cyclohexane (10 wt.%), 1-hexene (40 wt.%) and toluene (15 wt.%). For Fig. 9B case, the inlet fuel is composed of thiophene and *n*-heptane. It can be found that about 7 g and 14 g of the fuel has been desulfurized to below 0.1 mg L^{-1} sulfur using 1 g of MMMs, corresponding to the breakthrough and saturation capacity 4.6 and 8.6 mg S g^{-1} MMMs for Fig. 9A and B, respectively. The results indicated that the adsorption performance of MMMs decreased when various hydrocarbons added into inlet feed. The results can be explained by the competitive adsorption of thiophene and hydrocarbon, especially toluene, on the functional AgY particles embedded in MMMs. Both thiophene and toluene molecules interact with silver ions through π-complexation. The similar adsorption modes result in the reduced sulfur removal ability. Nevertheless, AgY zeolites maintain the preferential adsorption for thiophene, which is markedly related with the multiple types of adsorption sites on zeolites. The competing species adsorb differently in those distinct sites due to different electron property. The

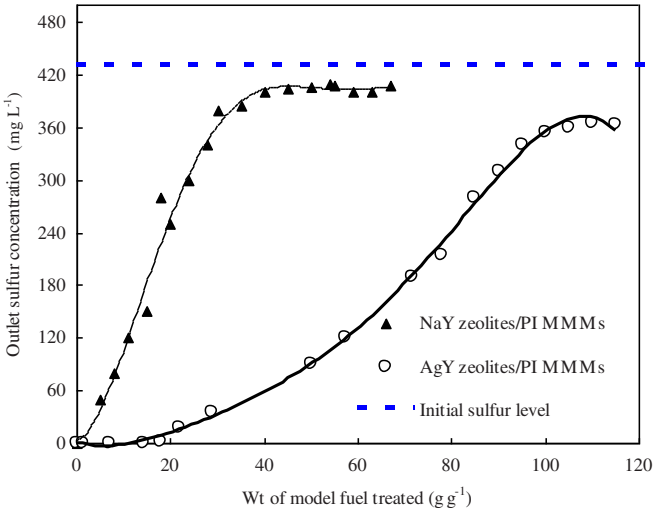

Fig. 8. Breakthrough curves for the adsorptive sulfur removal by MMMs.

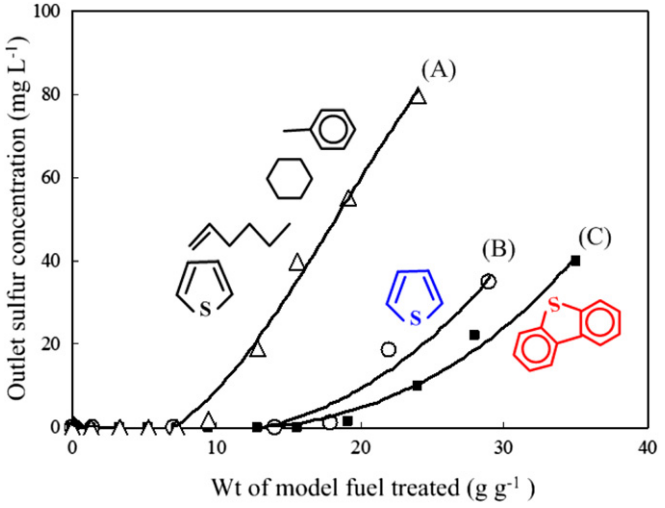

Fig. 9. Breakthrough curves of MMMs under various feed composition:(A) thiophene, *n*-heptane, cyclohexane, 1-hexene and toluene, (B) thiophene and *n*-heptane, (C) dibenzothiophene and *n*-octane.

conclusions have been verified by computational and experimental analysis [19–21].

Type of sulfur compounds in fuel is also important investigation subject for the desulfurization technology. Relevant research reveals that primary sulfur species in gasoline and diesel fuel are thiophenic sulfur compounds [22]. Fig. 9C shows the breakthrough curves and adsorption behavior of MMMs with feed containing dibenzothiophene (typical sulfur in diesel fuel). As depicted in Fig. 9C, the adsorption capacity (9.5 mg S g^{-1} MMMs) for dibenzothiophene is higher than that for thiophene, which is consistent with the higher electron density of S atoms for dibenzothiophene. The results suggest that the MMMs have higher desulfurization performance for diesel fuel. Based on molecular orbital calculations, Yang et al. [23] showed that the methyl groups in the substituted thiophenic compounds could enhance the electron back-donation process during π-complexation and, thus, resulted in the higher energies of adsorption.

3.4. Regeneration behavior

One of the challenging problems on adsorptive desulfurization is regeneration. Generally, there are two modes for regeneration of the spent MMMs, the solvent washing and the thermal treating. In this study, the solvent washing and thermal treating attempts both have been conducted for the spent MMMs incorporated with AgY zeolites, and the results are presented in Table 2. Experiment conditions are shown in the Experimental section.

From Table 2, the adsorption capacity of the MMMs decreases after the first regeneration, and then remains stable during the successive regenerations. Comparing with the fresh MMMs, the spent membranes can recover about 88% and 96% of the desulfurization capacity by solvent washing and thermal treating regeneration, respectively. In fact, the two kinds of regeneration mode have respective advantages. The solvent washing mode is convenient for on site operation during future scale-up of membrane adsorption process. It is well known that PI polymer has super solvent resistance and can be long-term used under solvent circumstances. That is one of the reasons why PI is selected as the matrix material in this study.

However, thermal treating mode shows higher regeneration efficiency. It is interesting to analyze the temperature resistance as well as the crystalline structure evolution during thermal treating of MMMs. The thermal properties of raw PI membrane, fresh MMMs and regenerative MMMs were characterized by DSC analysis, and the results are illustrated in Fig. 10.

From the DSC curves of Fig. 10, the melting temperatures (T_m) for raw PI membrane, fresh MMMs and regenerative MMMs are 521 °C, 526 °C and 527 °C, respectively. It is obvious that the MMMs have outstanding heat resistance, and the T_m of MMMs are higher than that of raw PI membrane. The interface interaction between organic PI material and inorganic zeolites restricts the thermal motion of

Table 2
The adsorption performance of regenerative MMMs.

Regeneration mode	Regeneration times	Adsorption capacity (mg S g^{-1})	Regeneration efficiency (%)
–	0	8.6	–
Solvent washing	1	7.7	89.5
Solvent washing	2	7.6	88.4
Solvent washing	3	7.4	86.0
Solvent washing	4	7.5	87.2
Thermal treating	1	8.3	96.5
Thermal treating	2	8.2	95.3
Thermal treating	3	8.4	97.7
Thermal treating	4	8.3	96.5

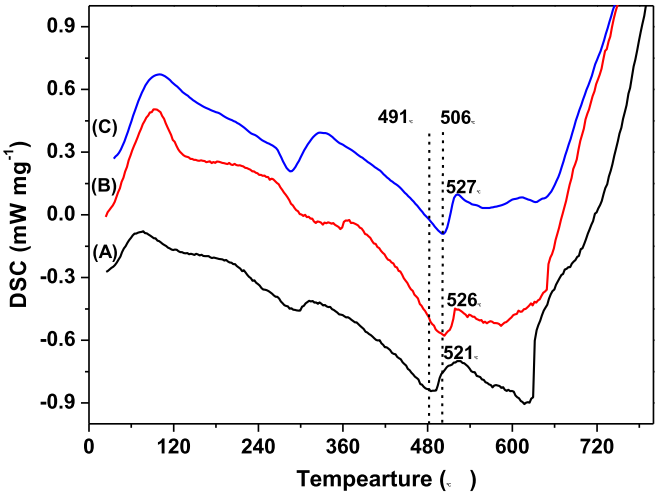

Fig. 10. DSC curves of raw PI membrane (A), fresh MMMs (B) and regenerative MMMs (C).

polymer chains, and increases the needed energy for the segmentation of polymer chains, which means the enhanced thermal stability of MMMs. The incorporation of crystalline zeolites into organic PI matrix also results in the increased crystallization temperature (T_c) as is shown in Fig. 10. Further XRD analysis has been conducted, and the XRD patterns of zeolites, MMMs, regenerative MMMs and PI membrane are presented in Fig. 11 and Fig. 12, respectively. Typical diffraction peaks (A–V) of zeolites in bulk at 11.55°, 15.3°, 18.3°, 19.9°, 22.4°, 23.2°, 24.7°, 25.3°, 26.5°, 27.3°, 28.8°, 30.2°, 30.8°, 31.9°, 32.6°, 33.5°, 34.1°, 35.2°, 37.2°, 38.7°, 40.1° and 40.7°, which show typical diffraction patterns of the Faujasite framework [24], are observed in Fig. 11. By comparative analysis on the XRD curves in Fig. 11, most of diffraction peaks (A*–Q*, S*, U* and V*) of zeolites can be clearly found in MMMs pattern, which indicates that the main framework structure of zeolites is maintained during embedding and encapsulation. The XRD pattern of raw PI membrane shown in Fig. 12 confirms a partly crystalline structure of PI with typical peaks at 14.1°and 17.8°, and the broad peak at around 20° is assigned to the amorphous phase. The crystalline peaks of PI matrix can also be found in the XRD patterns of MMMs. However, the hybridization of inorganic zeolites and organic PI matrix has certain effects on the order degree of MMMs

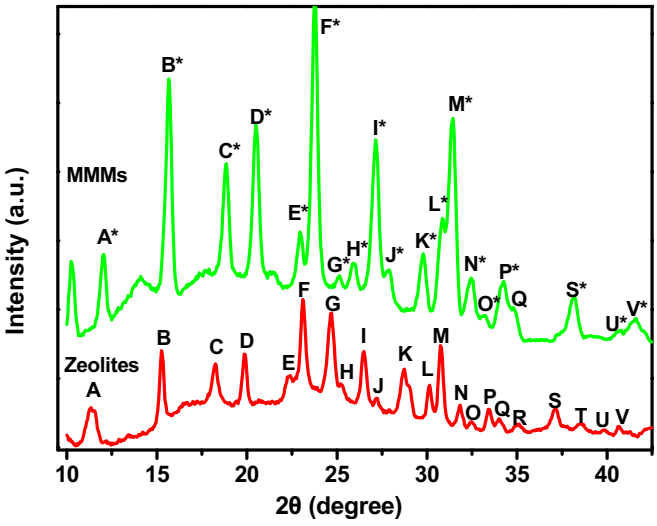

Fig. 11. XRD patterns of zeolites and zeolites/PI MMMs.

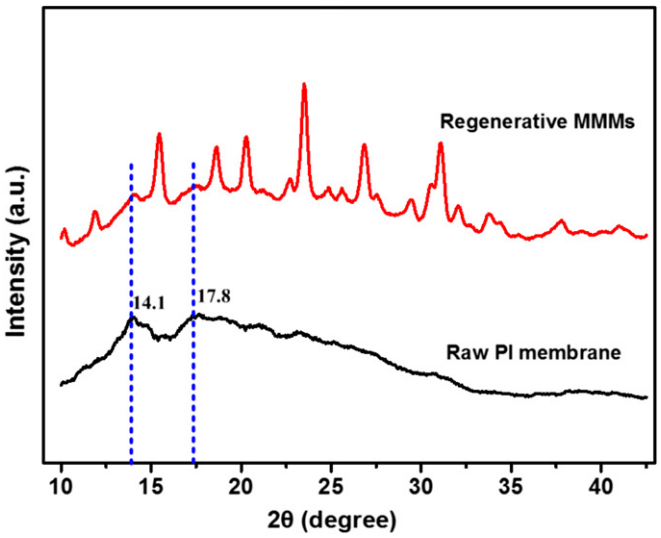

Fig. 12. XRD patterns of regenerative MMMs and raw PI membrane.

structure, leading to the difference of zeolite peaks in MMMs and in bulk. During hybridization process, the inevitable contraction and intersperse among certain pores and surface of zeolites with polymer chains result in the slight changes of aperture and channel of involved zeolites, which leads to the slight changes of relative peak intensity, disappearance of two weak peaks (peak R and T) and slight peak deviation (Fig. 11). Meanwhile, by comparative analysis on the XRD patterns of MMMs and regenerative MMMs in Figs. 11 and 12, it can be found that MMMs have similar patterns before and after regeneration by thermal treating under 250 °C, which demonstrates that the zeolite framework structure can be retained during thermal regeneration. The adsorption performance of regenerative MMMs maintained at high level compared with original MMMs (Table 2), which corresponds to the XRD analysis.

In summary, the prepared MMMs can be regenerated effectively. The excellent solvent resistance and heat resistance of PI matrix are significant for the regeneration process. The optimization and combination of the two kinds of regeneration mode are requisite in the future work for technology scale-up.

4. Conclusions

Membrane-based separations have great potential for applications to energy and environmental systems. In this paper, we have fabricated MMMs to discuss how the microporous channels facilitate the sulfur removal for fuel cell applications. Because the fuels under discussion are typical organic mixtures, and the methods used are quite general, the work can create opportunities to stimulate the application of MMMs on the separation of organic–organic mixtures. Most liquid pairs in this category are of industrial importance. Specifically, we believe that at least three aspects of this work will make it interesting to readers.

Firstly, the detailed analysis on the structure transition from finger-like to sponge-like gives the relationship among architecture conditions, transport channels and adsorption behavior. Appropriate retaining finger-like pores into the three-dimensional network structure of MMMs is favorable for achieving higher adsorption performance and flux. Secondly, the regeneration behavior of MMMs was discussed with two kinds of typical regeneration modes. High regeneration efficiency and sound reusability were obtained. Regeneration is a challenging problem on adsorptive material. The related discussions can provide helpful general suggestions.

Finally, the designed MMMs demonstrate effective sulfur removal property, which provides a potential alternative way for sulfur-free hydrogen source. The efforts are likely to play an influential role for the development of fuel cell area. Fuel cell is one of the most promising energy conversion devices for generating electricity. Especially for the automotive fuel cells and military fuel cells, liquid hydrocarbon fuels are ideal fuels due to their higher energy density, ready availability, and proven safety for transportation and storage. The hydrocarbons fuels can be converted to hydrogen for fuel cell applications relatively easily via steam reforming process, etc. To solve the poisoning of sulfur compounds in hydrocarbon fuels on the catalysts used in fuel cell system, the novel MMMs have been explored in this work. The exploited membrane approach shows superiority such as high efficiency, ease of on-board implementation, ambient operating conditions and ease of integration with fuel cell systems. The size of membrane adsorber is flexible, thus allowing it to be constructed for fuel cell modules under various scales. Sulfur is a severe poison for catalysts in fuel processors for fuel cells, especially reformer. The proposed MMMs adsorption adsorber may be applied as sulfur trap before the reformer for fuel cells on-board or on-site, and it may be applied in a periodically replaceable form. Further improvement in adsorption capacity and further design of hollow fiber membrane adsorber are desired, and more efforts are in progress toward this direction in our laboratory.

Acknowledgments

The authors acknowledge support of this work by National Natural Science Foundation of China (No. 21006070) and Tianjin Natural Science Foundation, China (No. 11JCZDJC23700, No. 11JCZDJC21200). This project is also supported by Research Fund for the Doctoral Program of Higher Education (No. 20091201120002) and State Key Laboratory of Hollow Fiber Membrane Materials and Processes (Tianjin Polytechnic University).

References

[1] X.L. Ma, L. Sun, C.S. Song, Catal. Today 77 (2002) 107–116.
[2] X.W. Zhang, S.H. Chan, G.J. Li, J. Power Sources 195 (2010) 685–702.
[3] E. Ito, J.A. Rob van Veen, Catal. Today 116 (2006) 446–460.
[4] M.F. Ali, A. Al-Malki, B. El-Ali, Fuel 85 (2006) 1354–1363.
[5] M. Rashtchi, G.H. Mohebali, M.M. Akbarnejad, Biochem. Eng. J. 29 (2006) 169–173.
[6] Y. Wang, F.H. Yang, R.T. Yang, Ind. Eng. Chem. Res. 45 (2006) 7649–7655.
[7] D.L. Gin, R.D. Noble, Science 332 (2011) 674–676.
[8] R.D. Noble, J. Memb. Sci. 378 (2011) 393–397.
[9] M.A. Aroon, A.F. Ismail, T. Matsuura, Sep. Purif. Technol. 75 (2010) 229–242.
[10] M.E. Avramescu, Z. Borneman, M. Wessling, J. Memb. Sci. 322 (2008) 306–313.
[11] S. Mohanapriya, S.D. Bhat, A.K. Sahu, Energy Environ. Sci. 2 (2009) 1210–1216.
[12] S. Keskin, D.S. Sholl, Energy Environ. Sci. 3 (2010) 343–351.
[13] T.S. Chung, L.Y. Jiang, Y. Li, Prog. Polym. Sci. 32 (2007) 483–507.
[14] L.G. Lin, Y.Z. Zhang, H.Y. Zhang, J. Colloid Interface Sci. 360 (2011) 753–759.
[15] L.G. Lin, A.D. Wang, M.M. Dong, J. Hazard. Mater. 203–204 (2012) 204–212.
[16] F. Liu, N. Awanis Hashim, Y.T. Liu, J. Memb. Sci. 375 (2011) 1–27.
[17] R.T. Yang, A.J. Hernández-Maldonado, F.H. Yang, Science 301 (2003) 79–81.
[18] Y. Kong, L.G. Lin, J.R. Yang, J. Memb. Sci. (2007) 36–43.
[19] S. Velu, X.L. Ma, C.S. Song, Ind. Eng. Chem. Res. (2003) 5293–5304.
[20] M. Xue, R. Chitrakar, K. Sakane, J. Colloid Interface Sci. (2005) 487–492.
[21] F.P. Tian, W.C. Wu, Z.X. Jiang, J. Colloid Interface Sci. 301 (2006) 395–401.
[22] A. Stanislaus, A. Marafi, M.S. Rana, Catal. Today 153 (2010) 1–68.
[23] F.H. Yang, A.J. Hernandez-Maldonado, R.T. Yang, Sep. Sci. Technol. 39 (2004) 1717–1732.
[24] M. Xue, R. Chitrakar, K. Sakane, J. Colloid Interface Sci. 298 (2006) 535–542.